Toward detecting atherosclerosis using dynamic laser speckle contrast imaging
A numerical study

Van As, K.; Dellevoet, S. F.L.J.; Boterman, J.; Kleijn, C. R.; Bhattacharya, N.; Kenjeres, S.

DOI
10.1063/5.0085411

Publication date
2022

Document Version
Final published version

Published in
Journal of Applied Physics

Journal of Applied Physics

Toward detecting atherosclerosis using dynamic laser speckle contrast imaging: A numerical study

Cite as: J. Appl. Phys. **131**, 184902 (2022); https://doi.org/10.1063/5.0085411
Submitted: 16 January 2022 • Accepted: 26 April 2022 • Published Online: 12 May 2022

K. van As, S. F. L. J. Dellevoet, J. Boterman, et al.

Journal of Applied Physics ARTICLE scitation.org/journal/jap

Toward detecting atherosclerosis using dynamic laser speckle contrast imaging: A numerical study

Cite as: J. Appl. Phys. **131**, 184902 (2022); doi: 10.1063/5.0085411
Submitted: 16 January 2022 · Accepted: 26 April 2022 ·
Published Online: 12 May 2022

K. van As,[1,2,a)] S. F. L. J. Dellevoet,[1] J. Boterman,[1] C. R. Kleijn,[1,2] N. Bhattacharya,[3,b)] and S. Kenjeres[1,2]

AFFILIATIONS

[1]Delft University of Technology, Faculty of Applied Sciences, Department of Chemical Engineering, 2629 HZ Delft, The Netherlands
[2]JM Burgerscentrum for Fluid Mechanics, 2628 CD Delft, The Netherlands
[3]Delft University of Technology, Faculty of Mechanical, Maritime and Materials Engineering, Department of Precision and Microsystems Engineering, 2628 CD Delft, The Netherlands

[a)]**Author to whom correspondence should be addressed:** K.vanAs@tudelft.nl
[b)]N.Bhattacharya@tudelft.nl

ABSTRACT

The disease atherosclerosis causes stenosis inside the patient's arteries, which often eventually turns lethal. Our goal is to detect a stenosis in a non-invasive manner, preferably in an early stage. To that end, we study whether and how laser speckle contrast imaging (LSCI) can be deployed. We start out by using computational fluid dynamics on a patient-specific stenosed carotid artery to reveal the flow profile in the region surrounding the stenosis, which compares well with particle image velocimetry experiments. We then use our own fully interferometric dynamic light scattering routines to simulate the process of LSCI of the carotid artery. Our approach offers an advantage over the established Monte Carlo techniques because they cannot incorporate dynamics. From the simulated speckle images, we extract a speckle contrast time series at different sites inside the artery, of which we then compute the frequency spectrum. We observe an increase in speckle boiling in sites where the flow profile is more complex, e.g., containing regions of backflow. In the region surrounding the stenosis, the measured speckle contrast is considerably lower due to the higher local velocity, and the frequency signature becomes notably different with prominent higher-order frequency modes that were absent in the other sites. Although future work is still required to make our new approach more quantitative and more applicable in practice, we have provided a first insight into how a stenosis might be detected *in vivo* using LSCI.

I. INTRODUCTION

The prevalence of atherosclerosis in the human species has been recorded right from pre-agricultural hunter–gatherer populations. In the carotid artery, the presence of atherosclerotic plaque causes stenosis, which increases the risk factor for ischemic stroke or transient ischemic attacks. The common non-invasive ways of examining a patient for carotid artery stenosis are magnetic resonance angiography and computed tomographic angiography,[1] which require expensive equipment. Ultrasound techniques, like duplex ultrasonography[1] and photoacoustic imaging,[2] may also be used; although being non-invasive, they offer different levels of discomfort to the patient. One optical technique that shows promise in providing an alternate way to screen patients is laser-speckle-based blood flow monitoring.

Speckle is the random interference pattern that arises when coherent light illuminates diffuse media and meets at the detector plane with varying path-length differences due to different trajectories traversed in the media. The speckle pattern contains useful information about the dynamics of the scatterers, because any motion of, or inside, a medium affects the speckle pattern. Speckle correlation is maintained when all scatterers have the same vectorial velocity and, thus, maintaining all inter-particle distances ("translating speckle"), but decorrelates due to the relative motion of the scatterers ("speckle boiling").[3]

Specifically for blood flow embedded in tissues, each of the layers that the light travels through affects the detected light by the varying transmission, reflection and absorption properties. Furthermore, each patient will be different, e.g., depending upon

health, age, and ethnicity of the patient. All these different scattering properties yield a static contribution to the measured speckle patterns. However, the temporal dynamics of the underlying flow or the moving scatterers will be imprinted in the temporal evolution of the speckle patterns, which may subsequently be studied.[4,5] A recent paper has used optical speckle image velocimetry to quantitatively reconstruct the velocity profile in blood vessels,[6] but their work is still invasive in nature. However, when using speckle patterns, no invasive imaging is necessary for the specific case of the carotid artery,[7] largely simplifying the required equipment. The latter makes speckle decorrelation a promising candidate as a technique to study the flow of turbid media,[8–10] such as blood.[11] However, to be able to derive useful information from speckle images, the physical process of light–tissue interaction needs to be studied first.

To that end, many different models have previously been used to study light propagation in tissues, such as simulating a photon random walk using the Monte Carlo technique,[12–14] approximating the light transport as a diffusive process,[15–19] or using the Mie–Percus–Yevick equations to model the scattering from blood.[20] For *in vivo* blood flow monitoring, there have been numerous studies based on speckle-based techniques, such as laser speckle contrast imaging (LSCI) and complementary techniques like multi-exposure LSCI.[7,21] In applications where direct imaging is possible, such as surface microvasculature, methods based on motion history image (MHI) analysis[22,23] or laser speckle optical flow imaging (LSOFI)[24] may be used. In principle, one should be able to quantitatively derive properties of the underlying flow from the measured speckle patterns (e.g., the velocity), even in cases where direct imaging is not possible such as deeper embedded vessels (e.g., the carotid artery). One metric that is affected by the speckle dynamics is the speckle contrast K that is simply the ratio of the intensity's standard deviation to its mean. Although it is now widely accepted in the literature that K scales inversely with velocity, the exact quantitative relationship still remains elusive.[25–28] Consequently, quantitative measurements still rely on combining multiple measurement techniques.[29] Nevertheless, with our goal of detecting atherosclerosis, we may bypass these challenges and use LSCI to qualitatively describe features of the underlying (blood) flow.

In our previous work, we had developed a new numerical procedure to simulate how a plane wave of monochromatic coherent light (i.e., a laser) scatters off of an ensemble of particles.[30] Our algorithm is based on the Mie theory, which gives the exact solution to how light scatters off of a sphere that we have then adapted to include multiple scattering. Although simplifications were made to make this approach computationally feasible, the advantage of our new approach is that we carefully track the phases. Consequently, we can simulate instantaneous speckle images containing all the interferometric information an experimental speckle pattern would also contain, allowing us to simulate the temporal dynamics, whereas the popular Monte Carlo approach yields statistical averages.[12] Using our new code, we had performed simulations using a sinusoidal- and a real heartbeat-modulated flow on both plug flow and Poiseuille flow in a cylinder. From the results, we have first shown that we could reconstruct the original heartbeat frequency from the dynamic speckle patterns. Then, we proceeded to show the effect of speckle boiling on the frequency spectrum of the speckles: speckle boiling caused by particles entering and leaving the laser beam and speckle boiling caused by the flow profile (i.e., Poiseuille flow) both have the effect of adding white noise[31] to the frequency spectra. When both origins of speckle boiling were present, their individual white noise effects added cumulatively. This is the primary advantage of performing simulations: we were able to simulate precise conditions that are unattainable in experiments, which allowed us to study the physics of speckle boiling in detail. The speckle boiling did not interfere with our ability to extract the original heartbeat frequency from the dynamic speckle, as we had obtained a signal-to-noise ratio of about 50.

In this work, we proceed to apply our computer model to the geometry of a carotid artery of a patient who suffers from atherosclerosis, i.e., there is a stenosis in the internal carotid artery. To that end, we have first coupled our light scattering code to an existing computational fluid dynamics code: OpenFOAM.[32] We then simulated the flow inside the artery and have compared our results to simulations performed in Ansys Fluent[33–35] and experimental results based on particle image velocimetry (PIV).[34,36] Finally, we simulated the light scattering in five different regions in the artery and we use LSCI and spectral analysis to study how we can detect a stenosis.

II. GENERIC APPROACH

The goal is to study atherosclerosis using LSCI (laser speckle contrast imaging). In LSCI, an object is illuminated by a laser (i.e., a plane wave of coherent monochromatic light), as is illustrated in Fig. 1. The light scatters off of all particles it encounters, and the scattered light is measured with a camera. Due to the interference of the scattered light with itself, a dynamic random interference pattern is formed as a result: a dynamic speckle pattern. Within the dynamic speckle pattern, information about the motion of the scatterers and thus the underlying flow system is contained.

We model this setup numerically, such that we can perform numerical experiments. We use a CT-scanned 3D model of an atherosclerosis patient's carotid artery[37] as our geometry (see Fig. 1). We use a computational fluid dynamics code to simulate the motion of tiny particles that represent red blood cells. A separate optics code simulates how the laser's light scatters off of these dynamic particles and mimics the measurement of a camera that has been placed at a right angle relative to the incoming light. Details of these two codes are discussed in Secs. III and V.

We perform numerical experiments on the artery at five different locations. These five sites are shaped cylindrically (i.e., the shape of the illuminated volume of a laser beam shining through), and they are at the following locations (see Fig. 2): nearby the inlet (A), right before the bifurcation (B), right before the sclerosed region in the internal carotid artery (C), inside the sclerosed region (D), and opposite of site C in the external carotid artery (E). The red circles in the figure show the location of the sites, as well as the size of the laser spot used. Details of this process are discussed in Sec. IV.

III. COMPUTATIONAL FLUID DYNAMICS

A. Approach

The fluid flow inside the artery is computed using a computational fluid dynamics (CFD) code. For our simulations, we have used the open source software OpenFOAM v2.4, and we validate

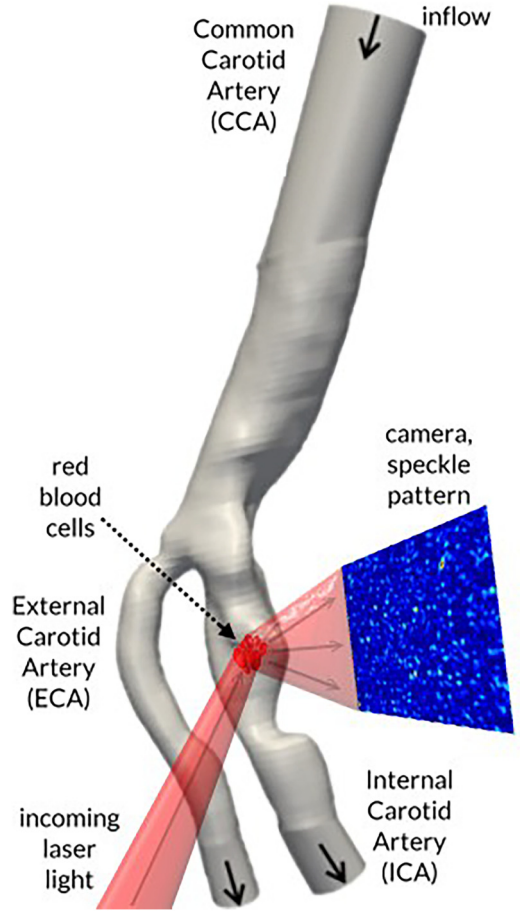

FIG. 1. Sketch of the laser speckle imaging process. Laser light hits an artery locally, scatters off of the flowing red blood cells, and forms a dynamic speckle pattern at a camera. The artery is a 3D model of a stenosed carotid artery.

our results to simulations performed in the proprietary CFD code Ansys Fluent[33–35] and experimental stereoscopic particle image velocimetry (PIV) results.[34,36] The arterial geometry is discretized using a tetrahedral mesh of 3.5×10^6 cells. In these cells, the incompressible Navier–Stokes equations are solved for the velocity and pressure fields using the finite volume method. These equations are combined using OpenFOAM's implementation of the PIMPLE algorithm with an iterative predictor–corrector method.[38] The convective terms are discretized using a second-order accurate linear upwind differencing scheme (LUDS), while the other spatial terms use a second-order accurate central differencing scheme (CDS). For the temporal discretization, the first-order Euler forward method is used with time step $\Delta t = 0.067$ s.

Many small (radius $4\,\mu$m) spherical particles are injected in the inlet to represent red blood cells. They are injected at a rate of 10^4 particles per second. Their motion in the computed fluid flow is calculated using Lagrangian particle tracking, in which we consider the small particles as perfect tracer spheres that do not affect

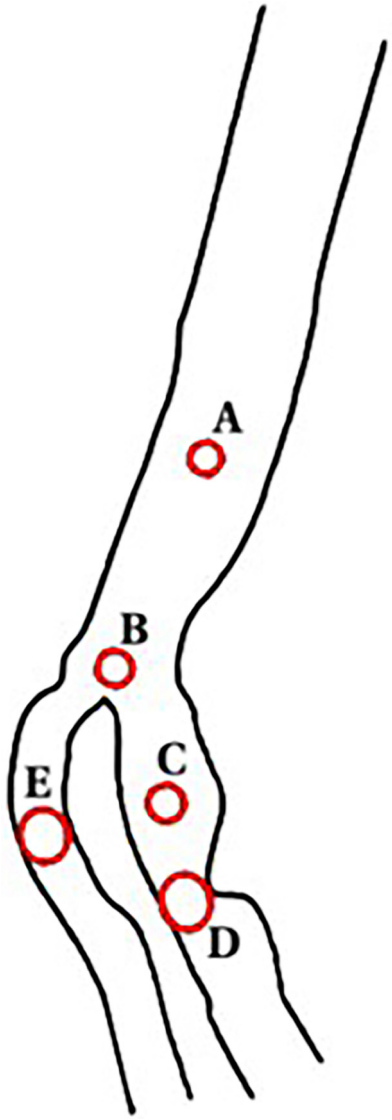

FIG. 2. The chosen sites on which we perform our numerical LSCI experiments.

the underlying flow. All physical parameters used in our CFD simulations are listed in Table I.

At the two outlets, we impose a fixed flow rate boundary condition for the velocity field, in which the flow rate at the two outlets is enforced to have the same ratio (60:40) as the outlet areas. At the arterial wall we impose a no-slip condition for the velocity and a zero normal gradient for the pressure. At the inlet of the common carotid artery, we impose a time-dependent flow rate $Q(t)$, such that the velocity u at the inlet is

$$\vec{u}(\vec{r}, t)|_{\text{inlet}} = -\frac{Q(t)}{A|_{\text{inlet}}} \nu(\vec{r})\hat{n}|_{\text{inlet}}, \quad (1)$$

TABLE I. Summary of the parameters relevant to CFD.

Kinematic viscosity fluid	$\nu = 8.28 \times 10^{-6}\ \mathrm{m^2/s}$
Density fluid	$\rho = 1157.2\ \mathrm{kg\,m^{-3}}$
Mean radius arterial inlet	$R\vert_{\mathrm{inlet}} = 9\ \mathrm{mm}$
Frontal area arterial inlet	$A\vert_{\mathrm{inlet}} = 2.63\ \mathrm{cm^2}$
Reynolds number at inlet	$\mathrm{Re}\vert_{\mathrm{inlet}} = 2\overline{u}R/\nu = 331.1$
Flow period	$T = 1.34\ \mathrm{s}$
Womersley number at inlet	$\alpha\vert_{\mathrm{inlet}} = 6.77$
Particle radius	$a = 4.00\,\mu\mathrm{m}$

where $A|_{\mathrm{inlet}}$ is the surface area of the inlet and $\hat{n}$ is the unit vector pointing outwards orthogonal to the surface area. At the inlet, we use the exact solution for flow inside an infinite cylinder (i.e., Poiseuille flow), $v(\vec{r}) = c(1 - r^2/R^2)$, which is a parabolic profile. R is the mean radius of the nearly-circular inlet, and the normalization constant c is chosen such that $v(\vec{r})$ integrates to unity over the inlet's surface area.

The input signal, $Q(t)$, and the extraction times[39] that we have used, is shown in Fig. 3. The signal is the same as the one used in the experiments that we compare our results in this section with. By the experimental limitations of the pump, the signal is not an exact heartbeat signal, but it does have the same distinct features such as a major oscillation followed by a minor oscillation.

Initially, we start with a zero velocity inside the entire artery. Several flow periods are needed for the entire flow to adapt to the inflow before a temporal equilibrium is reached, which takes a time, of the order of the flow-through time, for incompressible flow. To be on the safe side, we first simulate the flow for 10 periods before we start gathering any data for our simulations.

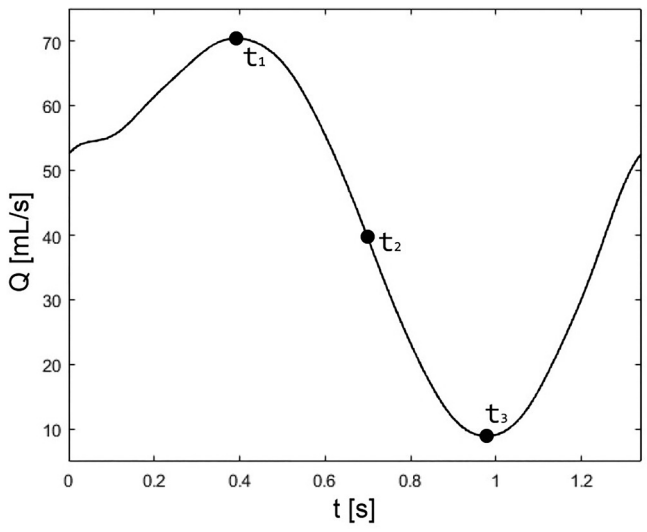

FIG. 3. The imposed flow rate at the artery's inlet, representing a simplified heartbeat signal. In this paper, we present flow results at the three labeled times, being at the maximum (t_1), the average (t_2) and the minimum (t_3) input flow rate.

Although real blood behaves as a non-Newtonian fluid due to the large particle density and the corresponding particle interactions, we use an incompressible Newtonian model to better match the experimental situation.[37] These experiments use PIV to obtain the velocity field inside the arterial geometry. The experimental artery was created by 3D-printing the arterial model, followed by casting a plastic phantom out of it. The scale compared to a real artery is approximately 21:10. The fluid was an aqueous glycerol solution seeded with hollow refractive-index-matched glass particles, varying in size between 2 and 20 μm diameter.

B. Results

The simulated flow profile at time $t = t_1$ (when the inlet velocity is maximum) is shown in Fig. 4(a) for two different slices.[40] The color scale indicates the velocity relative to the inlet velocity. There is a small stagnation point right above the bifurcation. The narrowing of the external carotid artery (ECA) results locally in a twice as high velocity. The same is true for the narrow stenosis in the internal carotid artery (ICA). Right before the stenosis is a region in which the velocity is lower, and in which local circulation forms. This is a characteristic flow pattern for detecting a stenosis.

At an average inlet velocity, such as is shown in Fig. 5(a), not much changes. The velocity relative to the inlet velocity is everywhere very similar. At the left side of the ICA, a streak starts to form, which becomes much more prominent at the lowest inlet velocity in Fig. 6(a). We presume that this is caused by the inertial forces of the preceding recirculation (i.e., the circular flow in the region right before the stenosis). That is, as the inlet velocity (V_0) decreases, the velocity (V) decreases everywhere, but the ratio V/V_0 does not decrease as fast directly adjacent to the recirculation.

A comparison with simulations performed in Ansys Fluent and with PIV measurements is shown in (b) and (c) of Figs. 4–6. Both simulations show the same flow features, both qualitatively and quantitatively. Although the resolution of the PIV measurements is less than that of the simulations, we can still see that the simulations have the same distinct flow features, and also match the velocity quantitatively in most spots. Figure 7 shows a more quantitative comparison along one specific cross-sectional line,[41] just after the bifurcation. In those figures, y^* is the zero-centered spatial coordinate along the line, normalized by the mean diameter of the arterial inlet. When comparing the ECA (i.e., $y^* < 0$ in Fig. 7), both simulations compare reasonably well with the PIV experiments; Fluent seems to perform better at a higher velocity ($t = t_1$), whereas OpenFOAM does so at lower velocities ($t = t_3$). In the ICA ($y^* > 0$), the PIV measurements deviate considerably. More specifically, the planar velocity inside the recirculation is lower in the PIV measurements and/or its recirculation region is larger. Since recirculation is rather sensitive to the local geometry, this may well be explained by manufacturing imperfections of the carotid artery mold used by the PIV experiments. Nevertheless, we expect that our fluid simulations are adequate for the laser speckle imaging conclusions we wish to draw in Sec. V.

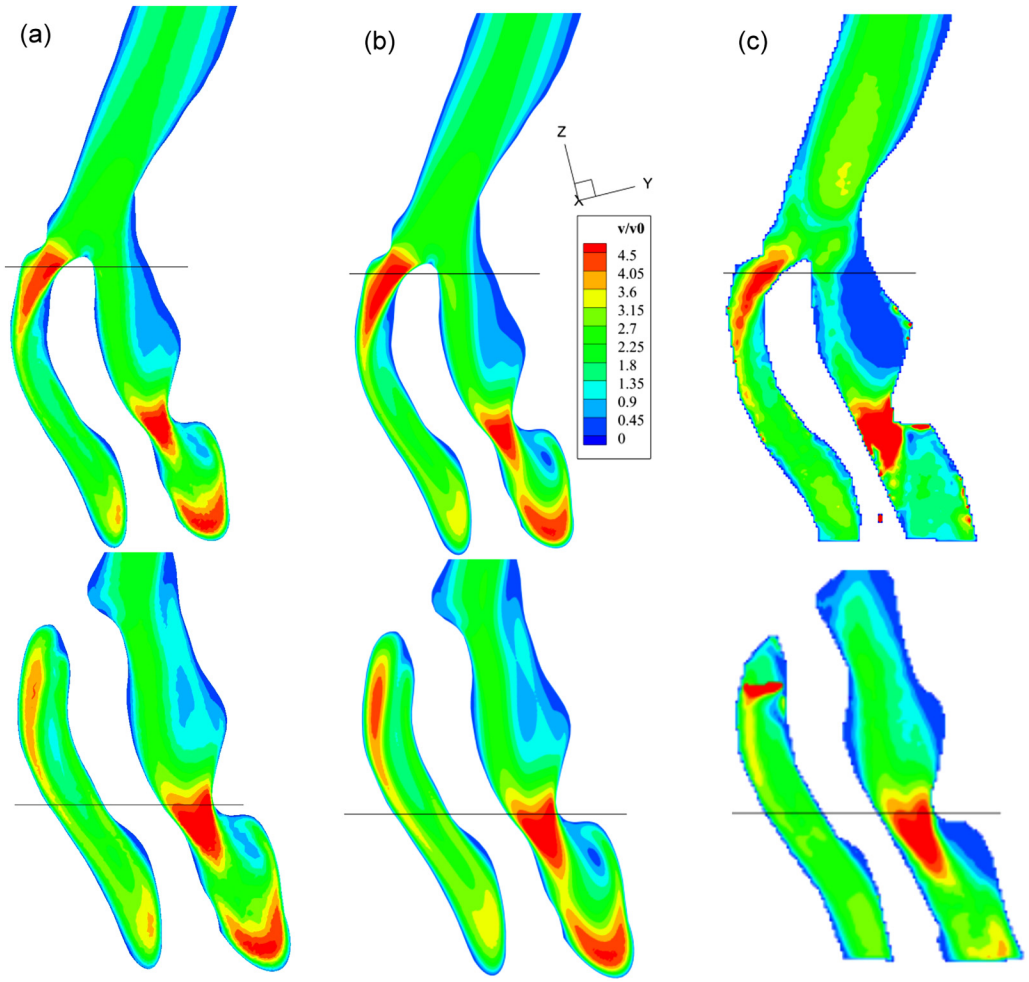

FIG. 4. Normalized flow profiles of the planar velocity V/V_0 at two different slices at maximum inlet velocity ($t = t_1$ in Fig. 3). Comparison between OpenFOAM simulations (a) Fluent simulations (b), and PIV experiments (c).

IV. COUPLING FLUIDS TO OPTICS

To study LSCI, we need to simulate how coherent light scatters off of the particles of which we calculated the motion in the previous section. This task will be performed by a separate optics code, which will be discussed in the next section. The advantage of using two separate codes, is that they are mutually independent: the optics code can use a set of particle positions as its input data, originating from any source—from any CFD simulation or experiment. However, the two codes will need to be coupled.

To that end, we extract the particle positions from our CFD simulations in the sites discussed in Sec. II. These sites are cylindrically shaped, to mimic a laser beam illuminating a subset of the total number of particles. The laser spot size was chosen such that there are on average approximately 100 particles within the illuminated volume. In that manner, a similar scattered light intensity may be expected on the camera for each numerical experiment. The extracted particle positions are then converted to the input format required by the optics code.

Only the particles that are directly inside the illuminated volume are extracted, and thus only they contribute to the (multiply) scattered light in our simulations. This only includes the small dynamic particles that were injected into the flow. In practice, one may expect a contribution by static scatterers inside the arterial wall and inside the tissue around it as well. When this will be incorporated in the future, one may expect the speckle dynamics to become more complex, manifesting in having additional frequency modes in the Fourier spectra.[42]

To study *dynamic* speckle imaging numerically, we deploy a trick. Each execution of the optics code is instantaneous, meaning we take the scatterers to be static while the light diffracts (i.e., the speed of light is "infinite" compared to that of the blood flow). To mimic the finite integration time t_{int} of a camera, which is a

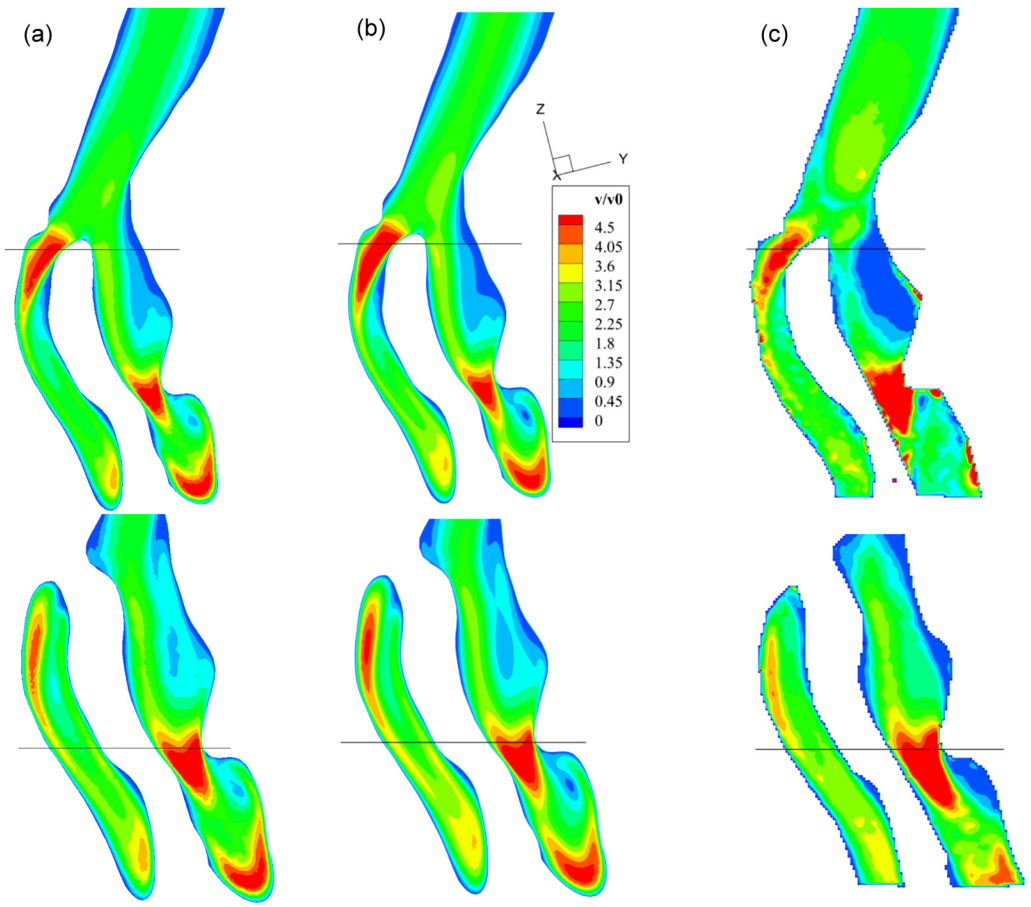

FIG. 5. Normalized flow profiles of the planar velocity V/V_0 at two different slices at average inlet velocity ($t = t_2$ in Fig. 3). Comparison between OpenFOAM simulations (a) Fluent simulations (b), and PIV experiments (c).

relevant parameter in dynamic LSCI,[25,26] we perform $n_{s,int}$ of such scattering simulations in very rapid succession.[30] This process is illustrated in Fig. 8. Finally, all simulated intensities are summed to obtain one single (blurred) speckle image. We call this process "microstepping." This process is then repeated a short while (Δt) later repetitively at the data sampling rate, $f_s = 1/\Delta t$, in order to obtain temporal data. All settings (as are summarized in Table II) were chosen based on our previous results: the speckle contrast [see Eq. (2)] is sensitive to changes in scatterer velocity at our chosen camera integration time,[28] and the number of integration samples is a compromise between computational time and an ~1% numerical integration error.[30] Altogether, 400 scattering simulations are performed for each flow period.

However, to perform the microstepping, we must first acquire the particle positions at each of the short Δt_{int} intervals, required by the optics code. The time step in the CFD simulations was chosen such that the flow data are available at precisely the required rate (f_s). Then, for each time (Δt apart), the CFD simulation is restarted to simulate mere microseconds of flow progression with a time step $\Delta t_{int} = 2.5\,\mu s$ for a time period of t_{int}. Finally, all particle positions are extracted, and the optics code is executed repetitively.

V. SPECKLE IMAGING

A. Approach: Optics code description

Our in-house optics code, which has been previously described in detail in Ref. 30, is fully interferometric, includes multiple scattering, and is based on the Mie theory. The Mie theory describes the scattering of a monochromatic plane wave by a single homogeneous spherical particle.[43–46] Using a far-field assumption, the scattered wave of each scatterer behaves locally in a distant region as a plane wave again. This is valid in a sufficiently dilute system or in a system containing sufficiently small particles.[30] Although this assumption is not satisfied for true blood flow, it does enable us to incorporate multiple scattering, which otherwise would have been computationally infeasible due to its $O(N^3)$ numerical complexity, where N is the number of particles in the illuminated volume. During multiple scattering, each particle

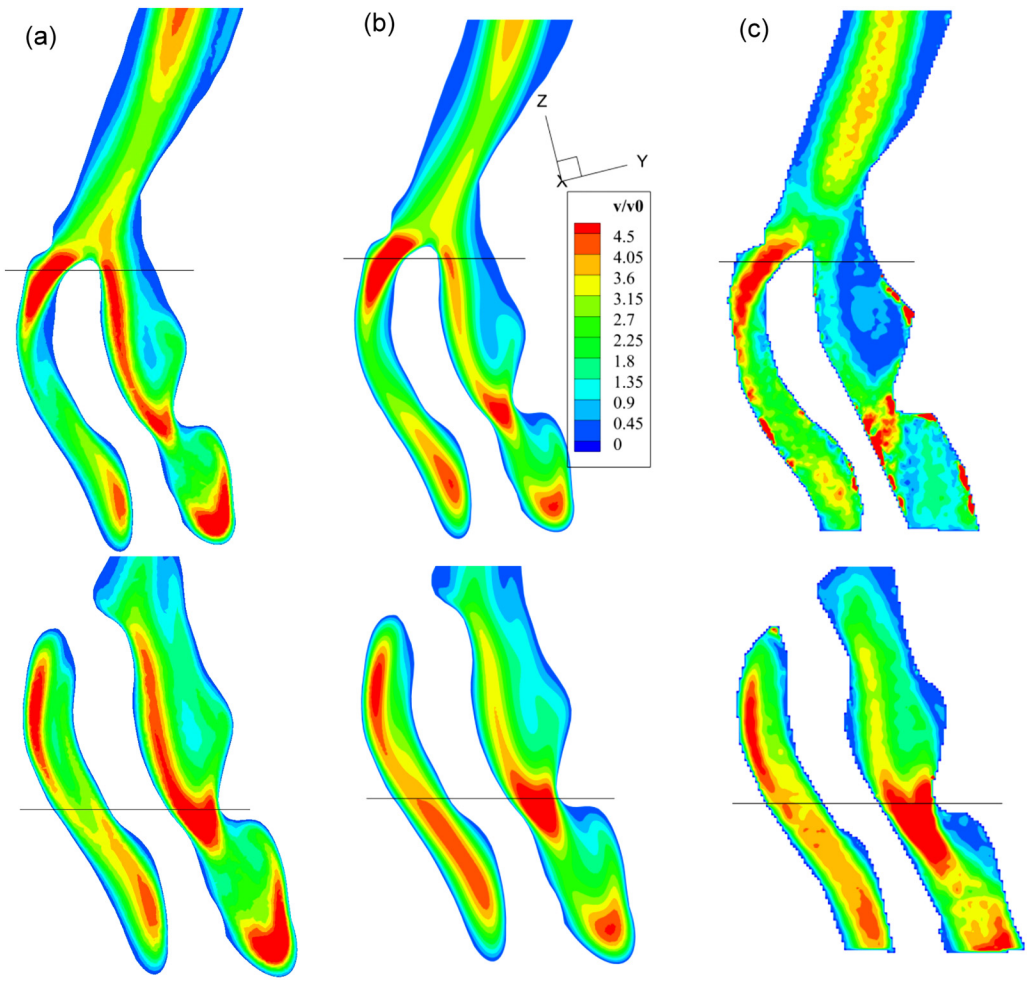

FIG. 6. Normalized flow profiles of the planar velocity V/V_0 at two different slices at minimum inlet velocity ($t = t_3$ in Fig. 3). Comparison between OpenFOAM simulations (a), Fluent simulations (b) and PIV experiments (c).

iteratively scatters to each other particle, including backscattering, until successive scattering orders contribute negligibly to the final result. Finally, all scattered light is added interferometrically at a two-dimensional grid of infinitesimal points (i.e., at our "camera"), and the intensity is computed by squaring the electromagnetic field. Note that no imaging system (such as lenses) is being simulated, as that is unnecessary to numerically obtain (dynamic) speckle images.

The assumptions made allow us to simulate dynamic laser speckle within a reasonable amount of time, while incorporating as much of the physics as possible. There exist alternative methods to our Mie calculation routine, such as the T-matrix method[47] which yield an exact result to the multiple scattering problem. However, since our dynamic simulations require $\mathcal{O}(10^4)$ instantaneous simulations, this is presently not practical with the available computational resources. Much more details about our code and its validity may be found in our previous paper.[30] The optics simulation parameters of the current work are summarized in Table III.

B. Approach: Post-processing speckle

An example of an instantaneous (simulated) speckle image is shown in Fig. 1. Within such speckle images, information about the underlying scatterers is contained. One metric for quantifying that information is the speckle contrast,[27,48]

$$K = \frac{\sigma_I}{\langle I \rangle}, \tag{2}$$

where I is the intensity, σ_I denotes its (spatial) standard deviation, and $\langle I \rangle$ is the mean (spatial) intensity. For fully developed (instantaneous) speckle, the speckle contrast is theoretically precisely[49]

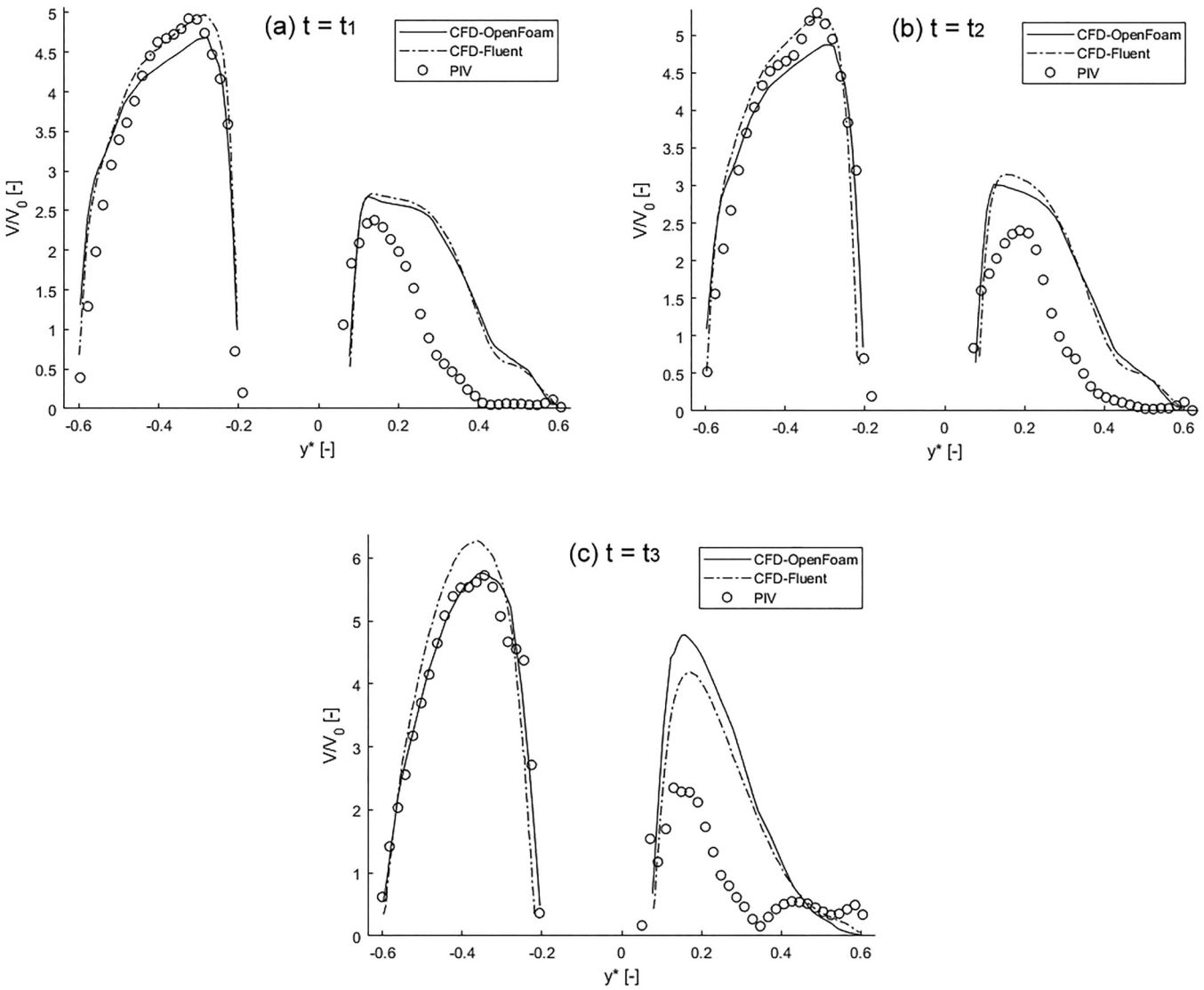

FIG. 7. Velocity profile along the cross-sectional line shown in the top figures of Figs. 4–6. y^* is the zero-centered spatial coordinate along the line, normalized by the mean diameter of the arterial inlet. The profiles are shown at maximum inlet velocity (a), at average inlet velocity (b) and at minimum inlet velocity (c).

$K = 1$. However, when light depolarizes due to multiple scattering such as is the case in tissues, K will become less than one.[50]

However, as the scatterers move, we do not obtain instantaneous speckle, but rather slightly blurred speckle patterns due to the finite integration time of the camera (see Sec. IV). The blurring causes σ_I to decrease, while not affecting $\langle I \rangle$, yielding a speckle contrast value $K < 1$. The amount of blurring is directly correlated with the velocity of the scatterers; thus introducing a dependency of K on the velocity of the underlying flow system, which makes K a useful metric for studying a flow system using dynamic speckle imaging.

Unfortunately, a truly quantitative relation between K and the velocity remains elusive.[25,51] In ideal situations, the model that assumes Gaussian statistics for the autocovariance of the temporal speckle fluctuations seems to perform well.[25,28] However, in realistic situations K is affected by disturbances, such as the speckle boiling caused by the scatterers entering/leaving the imaging plane (i.e., out-of-plane motion) and entering/leaving the illuminated volume. The speckle contrast is also bound to a minimum value due to the influence of static scatterers[26] and the influence of multiple scattering. Therefore, any quantitative measurement with laser speckle contrast imaging currently requires calibration.[26] Fortunately, K is still very useful for relative measurements: i.e., we might not know the precise velocity, but we can observe changes and differences, which gives us information about the underlying flow.

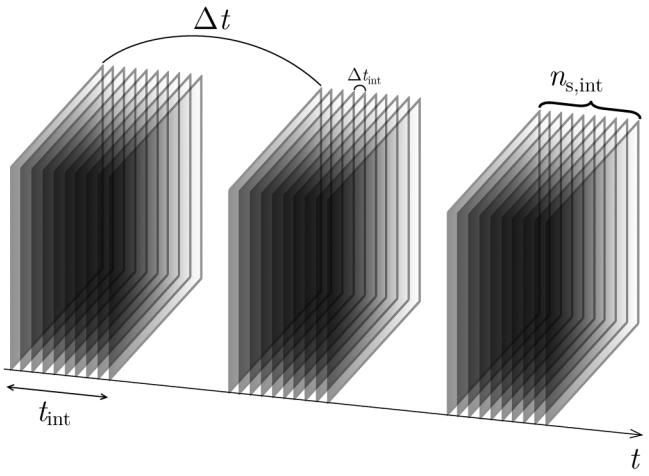

FIG. 8. To mimic the integration time of a camera, we sample instantaneous data at a short interval Δt_{int}. This process is repeated at distant intervals (Δt apart) to obtain temporal data (figure reprinted from our previous paper[30]).

To that end, we should first obtain accurate values of K. Due to the existence of large-scale interferometric fringes, we cannot simply compute K over the entire image, as those fringes arbitrarily increase σ_I and therefore K. These fringes are the consequence of our rather dilute simulations,[30] but the following has been reported to be relevant for experiments just as well.[52] The solution is to use *local* speckle contrast analysis (LSCA), in which the image is first subdivided in a total of $N_x \times N_y$ tiny square windows, then $K_{i,j}$ is computed in each subdivision, and finally K is simply the average of all $K_{i,j}$,

$$K = \frac{1}{N_x N_y} \sum_{i=0}^{N_y-1} \sum_{j=0}^{N_x-1} K_{i,j}. \tag{3}$$

We had found previously that for our simulated 128×128 pixels camera (see Table III), windows of about 8×8 pixels each yielded the best results for our simulations, with a maximum convergence error of $\sim 2.6\%$.[30]

Finally, we study *dynamic* speckle patterns, meaning we can compute K at our data sampling rate f_s (see Table II). The result is a time series $K(t)$ which contains information about the flow dynamics. Since we study flow in the carotid artery, it is prevalent

TABLE II. Summary of the simulation parameters relevant to data acquisition.

Total simulation time	35 periods
Data sampling rate	$f_s = 20$ samples/period
—corresponding frame rate (FPS)	$\simeq$26.8 Hz
Camera integration/exposure time	$\Delta t_{\text{int}} = 50\,\mu$s
No. integration samples	$n_{\text{s,int}} = 25$
Velocity of extracted particles	range: 0–1.2 m/s

TABLE III. Summary of the optics parameters.

Refractive index	$n_{\text{sphere}} = 1.52$ $n_{\text{medium}} = 1$
Wavelength	$\lambda = 532$ nm
Particle radius	$a = 4.00\,\mu$m
No. of pixels (camera)	$M = 128 \times 128$
Physical size of the camera "chip"	1.5×1.5 mm^2
Distance artery $\leftrightarrow$ camera	25 cm

that the periodicity of the heartbeat should reflect in the $K(t)$ signal as well. Therefore, it is also useful to calculate the frequency spectrum of $K(t)$ using the FFT; however, it should be noted that the frequency spectrum of $K(t)$ will not equal the frequency spectrum of the underlying velocity, since $K(t)$ does not scale linearly with velocity.[25,28] Rather, the frequency spectrum of $K(t)$ will have roughly the same major (i.e., first-order and second-order) frequency modes as the frequency spectrum of the velocity, but it will have additional higher-order frequency modes due to the non-linearity of the relationship.[30]

C. Results

The speckle contrast K was computed in each of the five sites (see Sec. IV) over the course of 35 flow periods (see Table II). The resulting frequency spectra are shown in Fig. 9 for each site, with the original speckle contrast time series shown in the inset of each figure. For quick reference, the input signal (flow rate Q vs time t) is shown in Fig. 9(a), together with an inset showing the location of each of the five sites.

Site A [see Fig. 9(b)] is just a little downstream of the inlet. In this region, the flow is still behaving nicely as there are no physical obstructions. Therefore, you would expect a rather clean signal that closely represents the inflow function, $Q(t)$.

However, speckle contrast K does not scale linearly with velocity v and thus not linearly with flow rate Q either. Rather, a low K corresponds with a low standard deviation of the intensity pattern σ_I, which implies that over the course of the camera integration time Δt_{int} much blurring occurs. In turn, this implies a high velocity v; therefore, a high v corresponds to a low K. Consequently, the time series (shown in the insets) paint an upside-down image of the local mean velocity.

When a Gaussian autocovariance of the temporal fluctuations is assumed, an equation for the relation between K and the speckle decorrelation time τ_c may be derived[25] that compares reasonably well with our previous simulations.[28] However, there is no agreement in the literature how to convert τ_c into velocity v, making the exact relationship elusive.[25,51] Regardless, we have found previously from simulating a sine input signal (which is just a single peak in the frequency spectrum) that the frequency spectrum of the speckle contrast time series has higher-order peaks at multiples of the dominant frequency.[30] These higher-order frequencies are caused by the non-linear relationship between K and velocity v that manifests in the broadening of the troughs and narrowing of the crests of $K(t)$ relative to the input signal. Consequently, it is not useful to directly compare the frequency spectra of K to the frequency

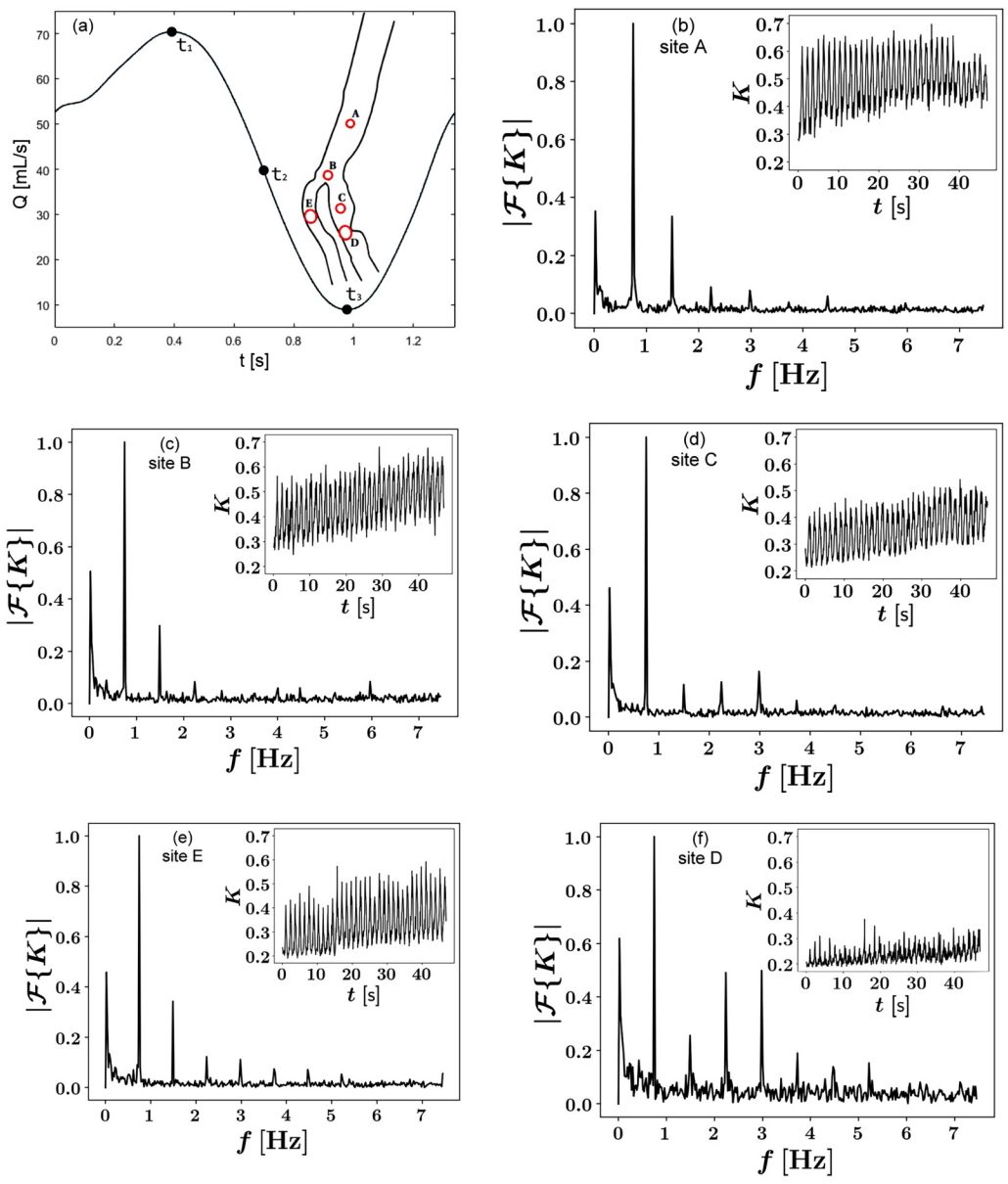

FIG. 9. Speckle contrast time series (inset) and its frequency spectrum (main figure) for each of the five sites. In (a), the (0.75 Hz) input signal of Fig. 3 and the location of the five sites in its inset from Fig. 2 is reproduced for quick reference. In (b)–(f), the five frequency spectra are ordered according to their location in the artery.

spectrum of the input signal.[53] Instead, we will compare all sites with site A, as site A is located just a little downstream of the inlet, where the flow is not yet disturbed.

In the frequency spectrum of site A [see Fig. 9(b)], the dominant frequency peak is at 0.75 Hz, which corresponds to the flow period (see Table I). There are also higher-order frequency peaks at multiples of the main frequency, partly due to the complex input signal and partly due to the non-linear relationship between K and velocity v. There is an additional peak at the near-zero frequency, which is also present for all other sites. This is merely a simulation artefact in OpenFOAM caused by particles getting stuck inside the walls (thereby slowly increasing the number of particles inside the illuminated volume), and should thus be ignored when studying the dynamic evolution of speckle. Finally, between all peaks there is noise that is not present in the input signal. In our previous work,[30] we have proven that this noise is fully caused by speckle

boiling due to the relative motion between the particles (i.e., the flow profile inside an artery is more like Poiseuille flow than plug flow), and particles entering and leaving the illuminated volume. In the present work, there is an additional third cause of speckle boiling, being out-of-plane motion of particles.

Site B [see Fig. 9(c)] is located at the bifurcation of the artery. In this region, one would expect additional speckle boiling as there is more relative motion between the particles: some go left, and some go right. Relative to site A, this manifests as more noise that is mostly visible at the higher frequencies. In site B, there is also a larger particle buildup than in any other site due to the bifurcation (and the earlier-mentioned simulation artefact), but the sole effect is a larger peak at the near-zero frequency. In general, the signature of site B's frequency spectrum is very similar to that of site A: the ratio between the first-, second-, and third-order peaks is very close. The only indication that the flow at site B is different (i.e., it is a bifurcation) is the increased amount of noise due to speckle boiling.

Site E [see Fig. 9(e)] is in the external carotid artery. From the fluid dynamics results, it can be seen that the flow in this region is fairly normal: there is a Poiseuille-like flow profile without vortices and backflow. As a consequence, the signature of site E's frequency spectrum is very similar to that of site A as well: the main frequency mode is well-represented, and the higher-order frequency modes have the same relative peak height. Relative to site A, the velocity is higher at site E, which also nicely follows from the optics since a lower mean K is measured in site E. Therefore, the speckle measurement can detect the increased velocity and the normal flow profile in site E.

Site C [see Fig. 9(d)] is the equivalent of site E, but in the internal carotid artery. The mean velocity in site C is similar to that in site E (see Figs. 4–6), which results in similar values for K. Like in site E, the main frequency mode is also well-represented. However, there are clear differences in the frequency signatures. The higher-order frequency modes are suppressed in site C, because its $K(t)$ does not have the expected broad troughs and narrow crests as much as the $K(t)$ of site E does have. This implies less extreme temporal velocity fluctuations in site C. From Figs. 4–6, it can be seen that there is a recirculation region (with backflow) in site C. The circulating flow's inertia acts as a buffer when the inflow velocity decreases, thus smoothing the crests of $K(t)$. Finally, the amount of noise (caused by speckle boiling) is similar in sites C, A, and E, which indicates a flow profile that behaves "nicely." Therefore, the same amount of noise in combination with the suppression of the second-order frequency mode might be characteristic for flow regions containing vortices/backflow.

Finally, site D [see Fig. 9(f)] is located inside the stenosis. First, the measured values of $K(t)$ are considerably lower than those in the other sites, which makes sense, because the center velocity in this region is roughly 4.5 times greater than the mean inflow velocity (see Figs. 4–6), which is roughly double the center velocity of the other sites. Second, the main frequency mode is still prominently visible, but the signal-to-noise ratio went down considerably. This is caused by the measured K being rather low, in which the sensitivity to changes in velocity v is low.[25,28] A better measurement may be performed by using a lower camera integration time Δt_{int}; however, we did not want to do that as we were interested in seeing what a (medical) device would measure when it would "scan" the artery without changing the device parameters. Third, the frequency signature is considerably different than in all other sites. As for the preceding site C, the second-order frequency mode is suppressed. Unique to site D is that the higher-order frequency modes actually became much more prominent, at least relative to the main frequency mode, as has also been found previously in experimental work.[37] Presumably, this is a downstream effect of the preceding unsteady flow region, which introduces flow features with a higher frequency as the unsteadiness causes the flow to no longer follow the input signal precisely. Therefore, characteristic for the stenosis are a lower K, more noise, a slightly suppressed second-order frequency mode, and more prominent higher-order frequency modes (relative to the main frequency mode).

VI. SUMMARY AND CONCLUSIONS

In this work, we set out to study atherosclerosis using dynamic LSCI (laser speckle contrast imaging), which should eventually result in the development of new medical measurement devices. To that end, we have developed a fully modular numerical routine to simulate dynamic LSCI of any flow system, comprising a separate fluid dynamics and a separate optics code that are subsequently coupled. The fluid dynamics code[54] simulates the flow and injected particles in an arbitrary geometry. The optics code is based on the Mie theory and uses the particle positions as its input to simulate how a coherent plane wave (i.e., a laser beam) scatters off of the ensemble of particles, including multiple scattering. The finite camera integration time of a real camera is mimicked by averaging over many instantaneous simulations at a short interval, thus providing us with blurred speckle that yields information about the dynamics of the underlying flow system. All speckle images are processed by computing the speckle contrast (for a duration of 35 flow periods) and its frequency spectrum, which we then study: "If this was an actual measurement of a (medical) device, can we detect specific flow features?"

We have applied our whole numerical routine to the case of a carotid artery suffering from atherosclerosis in the internal artery, to which a heartbeat-like input signal was applied. Our fluid dynamics simulations compare well with experiments. The velocity is higher in narrow regions, such as the stenosis. Directly downstream and upstream of the stenosis, there is a flow region with recirculation. Depending on the present input flow rate during the heartbeat cycle, the recirculation varies in strength. At the bifurcation of the artery, there is a stagnation point. In other parts of the artery, the flow behaves "nicely," with a Poiseuille-like flow profile.

We then used our optics code on five sites in the artery: (A) near the inlet, (B) at the bifurcation, (C) inside the recirculation and (D) in the stenosis in the internal artery, and (E) in the external artery. By comparing sites B and E to site A, we found virtually the same frequency signature, with just some more noise in site B caused by the bifurcation. In sites C and D, however, the frequency signature was different. Before the stenosis (site C), the noise remains unchanged, but the second-order frequency mode gets suppressed, presumably by the inertia of the circulating flow. Inside the stenosis (site D), the speckle contrast decreases rapidly due to the higher velocity, and the frequency signature changes

considerably: there is much more noise, and the higher-order frequency modes become more prominent while the second-order frequency mode is slightly suppressed. In other words, the signal is much more complex than in other regions in the artery due to the upstream recirculation before the stenosis, which spectral analysis of the speckle contrast is able to detect.

In conclusion, we have shown that more complex flow characteristics are reflected in the speckle contrast time series as obtained from dynamic LSCI. Therefore, spectral analysis of the speckle contrast can distinguish regions with complex flow. Consequently, the stenosis—and, thus, the disease atherosclerosis—can be detected with dynamic LSCI.

We are confident that our approach should be adaptable to *in vivo* situations, as we have previously used speckle imaging for an *in vivo* carotid artery.[7] To that end, future work should definitely study the region around the stenosis in more detail: what does the transition in frequency signature from upstream to all the way downstream of the stenosis look like precisely? Can we also detect the early stages of atherosclerosis in which the stenosis is not yet as large? Will the angle of measurement influence the results? And how will the patient's skin (i.e., static scatterers) affect the measurements? Finally, given the success of dynamic LSCI to detect flow features in our present context, it would be interesting to study many different kinds of flow to determine what other applications dynamic LSCI might have to study in particular flow systems that are currently difficult to measure, e.g., due to the opaque nature of said flow.

ACKNOWLEDGMENTS

The authors acknowledge the work of former M.Sc. students R. Li[35] and A. Muralidharan[36] on their preliminary CFD simulations and PIV experiments of the carotid artery.

This work was sponsored by the J. M. Burgerscentrum and the Netherlands Organisation for Scientific Research (NWO).

AUTHOR DECLARATIONS

Conflict of Interest

The authors have no conflicts to disclose.

DATA AVAILABILITY

The data that support the findings of this study are available from the corresponding author upon reasonable request.

REFERENCES

[1]J. F. Meschia, J. P. Klaas, R. D. Brown, Jr., and T. G. Brott, "Evaluation and management of atherosclerotic carotid stenosis," Mayo Clin. Proc. **92**, 1144–1157 (2017).
[2]P. Kruizinga, A. F. W. van der Steen, N. de Jong, G. Springeling, J. L. Robertus, A. van der Lugt, and G. van Soest, "Photoacoustic imaging of carotid artery atherosclerosis," J. Biomed. Opt. **19**, 1–3 (2014).
[3]T. Asakura and N. Takai, "Dynamic laser speckles and their application to velocity measurements of the diffuse object," Appl. Phys. **25**, 179–194 (1981).
[4]P. Zakharov, A. C. Völker, M. T. Wyss, F. Haiss, N. Calcinaghi, C. Zunzunegui, A. Buck, F. Scheffold, and B. Weber, "Dynamic laser speckle imaging of cerebral blood flow," Opt. Express **17**, 13904–13917 (2009).
[5]M. Heckmeier, S. E. Skipetrov, G. Maret, and R. Maynard, "Imaging of dynamic heterogeneities in multiple-scattering media," J. Opt. Soc. Am. A **14**, 185–191 (1997).
[6]M. M. Qureshi, Y. Liu, K. D. Mac, M. Kim, A. M. Safi, and E. Chung, "Quantitative blood flow estimation *in vivo* by optical speckle image velocimetry," Optica **8**, 1092–1101 (2021).
[7]M. Nemati, S. Kenjeres, H. Urbach, and N. Bhattacharya, "Fractality of pulsatile flow in speckle images," J. Appl. Phys. **119**, 174902 (2016).
[8]J. C. Dainty, "Laser speckle and related phenomena," in *Topics in Applied Physics* (Springer, 1975), Vol. 9.
[9]H. M. van der Kooij and J. Sprakel, "Watching paint dry: More exciting than it seems," Soft Matter **11**, 6353–6359 (2015).
[10]H. M. van der Kooij, R. Fokkink, J. van der Gucht, and J. Sprakel, "Quantitative imaging of heterogeneous dynamics in drying and aging paints," Sci. Rep. **6**, 2858 (2016).
[11]D. A. Boas and A. K. Dunn, "Laser speckle contrast imaging in biomedical optics," J. Biomed. Opt. **15**, 011109 (2010).
[12]A. J. Welch, M. J. C. van Gemert *et al.*, *Optical-Thermal Response of Laser-Irradiated Tissue* (Springer, 2011), Vol. 2.
[13]A. Sassaroli and F. Martelli, "Equivalence of four Monte Carlo methods for photon migration in turbid media," J. Opt. Soc. Am. A **29**, 2110–2117 (2012).
[14]M. A. Davis and A. K. Dunn, "Dynamic light scattering Monte Carlo: A method for simulating time-varying dynamics for ordered motion in heterogeneous media," Opt. Express **23**, 17145–17155 (2015).
[15]D. A. Boas, L. E. Campbell, and A. G. Yodh, "Scattering and imaging with diffusing temporal field correlations," Phys. Rev. Lett. **75**, 1855 (1995).
[16]M. A. O'leary, D. A. Boas, B. Chance, and A. G. Yodh, "Refraction of diffuse photon density waves," Phys. Rev. Lett. **69**, 2658 (1992).
[17]D. J. Pine, D. A. Weitz, P. M. Chaikin, and E. Herbolzheimer, "Diffusing-wave spectroscopy," Phys. Rev. Lett. **60**, 1134 (1988).
[18]M. J. Stephen, "Temporal fluctuations in wave propagation in random media," Phys. Rev. B **37**, 1 (1988).
[19]T. Durduran, R. Choe, W. B. Baker, and A. G. Yodh, "Diffuse optics for tissue monitoring and tomography," Rep. Prog. Phys. **73**, 076701 (2010).
[20]N. Bosschaart, G. J. Edelman, M. C. G. Aalders, T. G. van Leeuwen, and D. J. Faber, "A literature review and novel theoretical approach on the optical properties of whole blood," Lasers Med. Sci. **29**, 453–479 (2014).
[21]A. K. Dunn, "Laser speckle contrast imaging of cerebral blood flow," Ann. Biomed. Eng. **40**, 367–377 (2012).
[22]M. Z. Ansari, A. Humeau-Heurtier, N. Offenhauser, J. P. Dreier, and A. K. Nirala, "Visualization of perfusion changes with laser speckle contrast imaging using the method of motion history image," Microvasc. Res. **107**, 106–109 (2016).
[23]M. Z. Ansari and A. Mujeeb, "Application of motion history image (MHI) on dynamic fluorescent imaging for monitoring cerebral ischemia induced by occlusion of middle cerebral artery (MCA) in mouse brain," Biomed. Spectrosc. Imag. **6**, 135–142 (2017).
[24]A. Aminfar, N. Davoodzadeh, G. Aguilar, and M. Princevac, "Application of optical flow algorithms to laser speckle imaging," Microvasc. Res. **122**, 52–59 (2019).
[25]D. D. Duncan and S. J. Kirkpatrick, "Can laser speckle flowmetry be made a quantitative tool?," J. Opt. Soc. Am. A **25**, 2088–2094 (2008).
[26]D. Briers, D. D. Duncan, E. R. Hirst, S. J. Kirkpatrick, M. Larsson, W. Steenbergen, T. Stromberg, and O. B. Thompson, "Laser speckle contrast imaging: Theoretical and practical limitations," J. Biomed. Opt. **18**, 066018 (2013).
[27]A. F. Fercher and J. D. Briers, "Flow visualization by means of single-exposure speckle photography," Opt. Commun. **37**, 326–330 (1981).
[28]K. van As, B. A. Simons, C. R. Kleijn, S. Kenjeres, and N. Bhattacharya, "The dependence of speckle contrast on velocity" (unpublished).
[29]M. M. Qureshi, Y. Liu, K. D. Mac, M. Kim, A. M. Safi, and E. Chung, "Quantitative blood flow estimation in vivo by optical speckle image velocimetry," bioRxiv (2021).

[30]K. Van As, J. Boterman, C. R. Kleijn, S. Kenjeres, and N. Bhattacharya, "Laser speckle imaging of flowing blood: A numerical study," Phys. Rev. E **100**, 033317 (2019).
[31]That is, it is frequency-independent noise that may be filtered using Fourier analysis and a threshold filter.
[32]See http://www.openfoam.org/ for "The OpenFOAM Foundation" (2018).
[33]See https://www.ansys.com/products/fluids/ansys-fluent for "Ansys Fluent" (2018).
[34]S. Kenjereš, "On recent progress in modelling and simulations of multi-scale transfer of mass, momentum and particles in bio-medical applications," Flow Turbul. Combust. **96**, 837–860 (2016).
[35]R. Li, "Computational fluid dynamics methodology for simulation of blood flow in patient-specific carotid artery: Validation of two-dimensional three-components (2D3C) PIV," Master's thesis (TUDelft, Department of Chemical Engineering, 2017).
[36]A. Muralidharan, "*In-vitro* validation of cardiovascular flows using particle imaging velocimetry: A patient-specific validation study," Master's thesis (TUDelft, Department of Chemical Engineering, 2017).
[37]M. Nemati, G. Loozen, N. Van der Wekken, G. Van de Belt, H. Urbach, N. Bhattacharya, and S. Kenjeres, "Application of full field optical studies for pulsatile flow in a carotid artery phantom," Biomed. Opt. Express **6**, 4037–4050 (2015).
[38]J. H. Ferziger, M. Perić, and R. L. Street, *Computational Methods for Fluid Dynamics* (Springer, 2002), Vol. 3.
[39]The precise extraction time of the OpenFOAM simulation data differs slightly from Fluent and PIV due to OpenFOAM's dynamic timestepping, but this difference is insignificant for the comparison of the flow profiles.
[40]The top slice has origin (0.201, 0.1453, 0.3902) and normal vector (100, −0.5415, 0.3794). The bottom slice has origin (0.2054, 0.1389, 0.3455) and normal vector (−100, 1.3, −0.119). Note that these slices are basically just YZ-planes, but rotated ever so slightly to better correspond with the experimental orientation of the artery. TecPlot360X-2017 was used to extract the slices and plot the contours.
[41]The cross-sectional line is the intersection of the top slice (see Ref. 40) with the plane with origin (0.2007, 0.1407, 0.3690) and normal vector (0, −21.45, −97.67).
[42]M. Nemati, C. N. Presura, H. P. Urbach, and N. Bhattacharya, "Dynamic light scattering from pulsatile flow in the presence of induced motion artifacts," Biomed. Opt. Express **5**, 2145–2156 (2014).
[43]G. Mie, "Beiträge zur optik trüber medien, speziell kolloidaler metallösungen," Ann. Phys. **330**, 377–445 (1908).
[44]C. F. Bohren and D. R. Huffman, *Absorption and Scattering of Light by Small Particles* (John Wiley & Sons, 2008).
[45]J. A. Stratton, *Electromagnetic Theory* (John Wiley & Sons, 2007).
[46]H. C. Hulst, *Light Scattering by Small Particles* (Courier Corporation, 1981).
[47]M. I. Mishchenko, L. D. Travis, and D. W. Mackowski, "T-matrix computations of light scattering by nonspherical particles: A review," J. Quant. Spectrosc. Radiat. Transfer **55**, 535–575 (1996).
[48]J. D. Briers and S. Webster, "Laser speckle contrast analysis (LASCA): A non-scanning, full-field technique for monitoring capillary blood flow," J. Biomed. Opt. **1**, 174–180 (1996).
[49]J. W. Goodman, "Statistical properties of laser speckle patterns," in *Laser Speckle and Related Phenomena* (Springer, 1975), pp. 9–75.
[50]J. Li, G. Yao, and L. V. Wang, "Degree of polarization in laser speckles from turbid media: Implications in tissue optics," J. Biomed. Opt. **7**, 307–312 (2002).
[51]R. Bandyopadhyay, A. Gittings, S. Suh, P. Dixon, and D. J. Durian, "Speckle-visibility spectroscopy: A tool to study time-varying dynamics," Rev. Sci. Instrum. **76**, 093110 (2005).
[52]M. Draijer, E. Hondebrink, T. van Leeuwen, and W. Steenbergen, "Review of laser speckle contrast techniques for visualizing tissue perfusion," Lasers Med. Sci. **24**, 639 (2009).
[53]For this reason, we omit showing the input's frequency spectrum to prevent confusion.
[54]In our work, we have used OpenFOAM,[32] but in principle *any* computational fluid dynamics code may be used.